Available online at www.sciencedirect.com
ScienceDirect
Trans. Nonferrous Met. Soc. China 27(2017) 863−867
Transactions of Nonferrous Metals Society of China
www.tnmsc.cn

# Optical properties and magnetic properties of antisite-disordered $Ni_{1-x}Co_xCr_2O_4$ spinels

Yu GAO, Hong CHANG, Qiang WU, Hong-yan WANG, Yan-bo PANG, Fang LIU, Hong-jing ZHU, Yue-hou YUN

School of Physics, Inner Mongolia University, Hohhot 010021, China

Received 29 February 2016; accepted 8 July 2016

**Abstract:** From the UV−Vis absorption spectra, the FT-IR absorption spectra and the Raman spectra, it is deduced that Co ions primarily occupy the tetrahedral (A) site, with a minor number of them entering into the octahedral (B) site in the $Ni_{1-x}Co_xCr_2O_4$ compounds. The origin of the position disorder of the Co ions is consistent with the similar ionic radii of the Co ion (0.65 Å) and the Cr ion (0.62 Å) at B site. The FT-IR peak at about 510 $cm^{-1}$ shifts towards high frequency side with the increasing cobalt content. It is resulted from the reduction of the cation−oxygen distance in the octahedron by the replacement of the $Ni^{2+}$ with the $Co^{2+}$ ions. The magnetic measurement shows that Curie temperatures ($T_C$) are 75 and 90 K for the compounds with $x$=0.2 and 0.8, respectively.
**Key words:** spinel; antisite defect; electronic transition; optical properties; magnetic properties

## 1 Introduction

Chromium-based spinel-type compounds with a general formula $ACr_2O_4$ have received considerable attention due to their interesting magnetic properties and prospective applications [1,2]. For example, both of the $NiCr_2O_4$ and $CoCr_2O_4$ can be used as catalysts, gas sensors, pigment, and magnetic materials [3]. Cobalt chromite ($CoCr_2O_4$) crystallizes in cubic $Fd\bar{3}m$ space group and no structural phase transition is reported, while $NiCr_2O_4$ has a cubic $Fd\bar{3}m$ to tetragonal $I4_1$/amd phase transition caused by the Jahn–Teller distortion [4,5]. It is suggested that upon doping $NiCr_2O_4$ with Co ions, Co ions replace Ni ions at A site. The ionic radius of $Co^{2+}$ (0.58 Å) is greater than that of $Ni^{2+}$ (0.54 Å) at A site, which may explain the variation of cation−cation and ion−oxygen distances, and the distortion of tetrahedrons and octahedrons containing $A^{2+}$ and $Cr^{3+}$, respectively [4]. In single-crystal samples, collinear ferrimagnetic ordering occurs at $T_c$=93 K and 74 K for $NiCr_2O_4$ and $CoCr_2O_4$, respectively [6]. $CoCr_2O_4$ exhibits a multiferroic ordering below 26 K. In perfect normal $AB_2O_4$ spinel, $A^{2+}$ ions occupy the tetrahedral (A) site and $B^{3+}$ ions occupy the octahedral (B) site [4,7]. However, EWAIS et al [8] discovered that some A sites were occupied by $Al^{3+}$ ions and some B sites were occupied by $Mg^{2+}$ ions for $MgAl_2O_4$ spinel. GABAL et al [9] found that a half of the iron ions preferentially located at A sites and the others were at B sites, nickel ions and chromium ions occupied mostly B sites for $NiFe_{2-x}Cr_xO_4$. Therefore, a certain degree of disorder could occur in $ACr_2O_4$, i.e., some of the A site are occupied by $Cr^{3+}$ ions and some of the B site are occupied by $A^{2+}$. This departure from the normal spinel structure causes the antisite defect. These antisite defects play an important role in ion-surface interaction process and influence the electrical and optical behaviors of $ACr_2O_4$ spinel powders [8]. The $Ni_{1-x}Co_xCr_2O_4$ solid solution samples were studied by KOCHUR et al [4] using the method of X-ray photoelectron spectroscopy (XPS) and displayed that Ni ions occupied A sites and B sites and chromium ions located at B sites. In this work, we concentrate on studying the crystal structure, the locations of $Co^{2+}$, the optical properties and the magnetic properties of $Ni_{1-x}Co_xCr_2O_4$ with the X-ray diffraction (XRD) patterns, the Fourier transform infrared spectroscopies (FT-IR), UV-Vis spectra, Raman spectroscopy and magnetic property measurements.

**Foundation item:** Project (11264024) supported by the National Natural Science Foundation of China; Projects (2015MS0102, 2015MS0524) supported by Natural Science Foundation of Inner Mongolia, China
**Corresponding author:** Hong CHANG; Tel:+86-731-4993141; E-mail: changhong@imu.edu.cn
DOI: 10.1016/S1003-6326(17)60099-2

## 2 Experimental

Polycrystalline samples of $Ni_{1-x}Co_xCr_2O_4$ ($x$=0, 0.05, 0.1, 0.15, 0.2, 0.3, 0.5, 0.7, 0.8, 0.85, 0.9, 0.95 and 1.0) were prepared by solid-state reaction. The starting materials NiO, $Co_2O_3$ and $Cr_2O_3$ were ground in an agate mortar, heated at 850 °C in air for 12 h and then heated at 1150 °C in air for 48 h 2 times in order to ensure complete reaction. Powder X-ray diffraction (XRD) measurements were carried out using a RigakuD/max-2500 powder X-ray diffractometer with Cu $K_\alpha$ ($\lambda_1$=0.15406 nm and $\lambda_2$=0.15443 nm) radiation. The diffraction data were collected for structure analysis, and the scan range $2\theta$ was from 5° to 80°, with a scanning step of $2\theta$=0.014° and a sampling time 1 s. UV-Vis spectra were recorded in the 200−800 nm domain with a PerkinElmer Lambda750 UV-Vis spectrometer at room temperature. Fourier transform infrared (FT-IR) spectra were recorded with a NICOLET AVATAR 330 spectrometer in the range of 4000−400 $cm^{-1}$. The samples were mixed with KBr in the mass ratio of 1:200, and then were pressed into pellets. Raman spectra were recorded in the 100−900 $cm^{-1}$ domain with Renishaw inVia Laser confocal Raman spectrometer. Magnetization measurements were carried out on a Quantum Design superconducting quantum interference device (SQUID) magnetometer. Magnetization as a function of temperature was measured in the range of 5−200 K with an applied field of $4\times10^4$ A/m. Magnetization as a function of field was measured up to a maximum field of $5.57\times10^6$ A/m.

## 3 Results and discussion

### 3.1 XRD patterns

The XRD pattern shows that the $NiCr_2O_4$ has the tetragonal structure with the space group $I4_1/amd$. However, the structure of $Ni_{1-x}Co_xCr_2O_4$ with $x\geq0.05$ is cubic with the space group $Fd\bar{3}m$. Figure 1 shows the XRD patterns of $Ni_{1-x}Co_xCr_2O_4$ ($x$=0, 0.05) as representatives. The diffraction peaks shift to lower diffraction angles as $x$ increases, and it indicates that the lattice constant increases with the increasing cobalt content. This lattice expansion is due to the larger ionic radius of $Co^{2+}$ ($r$=0.58 Å) than that of $Ni^{2+}$ ($r$=0.55 Å) at the A site.

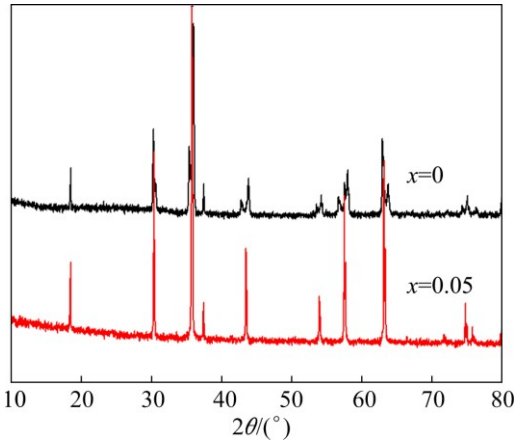


**Fig. 1** XRD patterns of $Ni_{1-x}Co_xCr_2O_4$ ($x$=0, 0.05) in range of $5°<2\theta<80°$

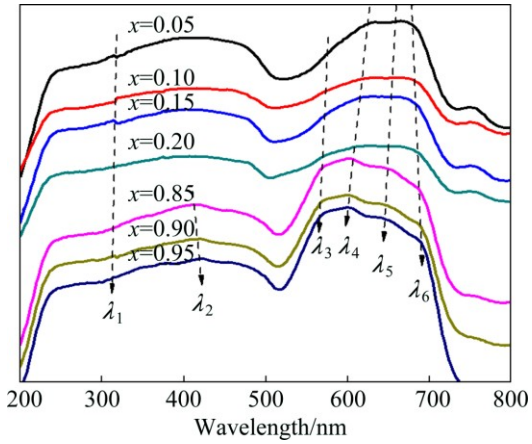


**Fig. 2** UV-Vis absorbance spectra of $Ni_{1-x}Co_xCr_2O_4$ ($x$=0.05, 0.1, 0.15, 0.2, 0.85, 0.9 and 0.95)

### 3.2 UV-Vis spectra

The UV-Vis reflectance spectra transform to the UV-Vis absorbance spectra with the formula $A=\lg(1/R)$, where $A$ is the absorbance factor and $R$ is the reflectance factor. Figure 2 shows the UV-Vis absorbance spectra of $Ni_{1-x}Co_xCr_2O_4$ ($x$=0.05, 0.1, 0.15, 0.2, 0.85, 0.9 and 0.95). The peak $\lambda_1$ at about 315 nm is due to a charge transfer between the cation and the oxygen at high energy. The absorption peaks, $\lambda_3$ at about 570 nm, $\lambda_4$ at about 610 nm and $\lambda_5$ at about 645 nm, are attributed to the spin-allowed electronic transition $^4A_2(F)\rightarrow{}^4T_1(P)$ of $Co^{2+}$ ions at the A site. The UV-Vis spectra of the compounds with $x\leq0.2$ have delicate charateristics, the comparatively weak peaks include $\lambda_3$ at about 570 nm and $\lambda_5$ at about 645 nm, while the peak $\lambda_4$ at about 610 nm is relatively strong. This illustrates that $\lambda_4$ at about 610 nm is assigned to not only the transition $^4A_2(F)\rightarrow{}^4T_1(P)$ of the high spin $Co^{2+}$ ion at the A site, but also the transition $^4A_{2g}\rightarrow{}^4T_{2g}$ of $Cr^{3+}$ ion at the B site. $\lambda_6$ at about 680 nm is attributed to the superposition of the spin forbidden transitions $^4A_{2g}\rightarrow{}^2T_{1g}$ and $^4A_{2g}\rightarrow{}^2E_g$ of $Cr^{3+}$ ions at the B site. A weak absorption peak, $\lambda_2$, appears at about 415 $cm^{-1}$ for the compounds with $x\geq0.85$, which is related to the spin-forbidden transition $^4A_2(F)\rightarrow{}^2T(G)$ of the Co ions at the B site, as reported by ZAYAT and LEVY [10]. In a perfect normal $ACr_2O_4$ (A=Ni and Co) spinel, the $A^{2+}$ ions occupy the A site and

$Cr^{3+}$ ions occupy the B site. However, $\lambda_2$ implies that some of the B sites are occupied by $Co^{2+}$ ions. The departure from the normal spinel structure causes the antisite defect. All the observed bands suggest that Co ions locate at both A and B sites, while Cr ions locate only at B site in $Ni_{1-x}Co_xCr_2O_4$. The origin of the antisite defect is probably due to the similar ionic radii of Co ions (0.65 Å) and Cr ions (0.62 Å) at the B site.

### 3.3 FT-IR spectra

The FT-IR spectra of $Ni_{1-x}Co_xCr_2O_4$ is shown in Fig. 3. There are two strong peaks at about 510 $cm^{-1}$ and 620 $cm^{-1}$, which are the characteristic peaks of the spinel and depend on the vibration of the cations at the B site [11]. Each oxygen ion in the spinel is shared by a cation at the A site and three cations at the B site. The replacement of small Ni ions by large Co ions at the A site leads to the increase of the A cation—O distance in the tetrahedron. As a compensation, it compresses the octahedron and results in a shrinking of the B cation—O distance in the octahedron, and increases the B cation—O bond energy. Consequently, the band at around 510 $cm^{-1}$ shifts towards the high frequency side with the increasing cobalt content. The intensity of the peak at about 600 $cm^{-1}$ is rather weak and delicate and it increases gradually with the increasing cobalt content. This indicates that some of the Co ions enter into the B site instead of the A site and confirms that the antisite defects exist in $Ni_{1-x}Co_xCr_2O_4$. Meanwhile, the peak at 600 $cm^{-1}$ shifts towards high frequency side with the increasing cobalt content. It has the same origin as the shift of the peak around 510 $cm^{-1}$ in the FT-IR spectra described above.

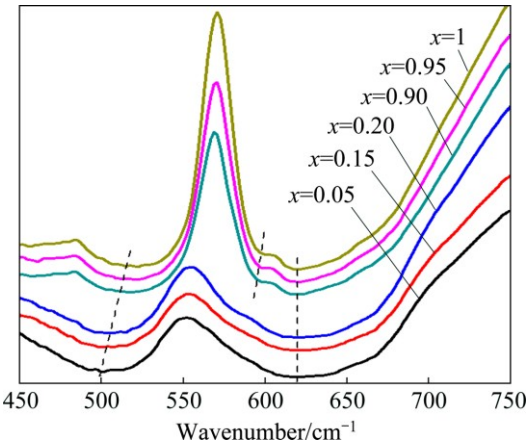


**Fig. 3** FT-IR spectra of $Ni_{1-x}Co_xCr_2O_4$ ($x$=0.05, 0.15, 0.2, 0.9, 0.95, 1.0)

### 3.4 Raman spectra

Raman spectra of the $Ni_{1-x}Co_xCr_2O_4$ ($x$=0.2 and $x$=0.8) samples are shown in Fig. 4. All the values of these peaks are listed in Table 1. According to group theory, the normal spinel have five Raman-active phonon modes ($\Gamma$=1$A_{1g}$+1$E_g$+3$F_{2g}$ or alternatively 3$T_{2g}$) [12,13], corresponding to the five peaks ($v_1$ ($T_{2g}$), $v_2$ ($E_g$), $v_3$ ($T_{2g}$), $v_4$ ($T_{2g}$), and $v_7$ ($A_{1g}$) ), respectively. The five peaks of the $Ni_{1-x}Co_xCr_2O_4$ samples shift to high frequency side with the increasing cobalt content. The increasing Raman-active phonon mode energy reflects that the doping Co ions tend to influence the tetragonal structure [12]. The peak $v_5$ is owed to the stretching modes of Cr—O—Cr [14]. Compared with the Raman spectra of $ZnCr_2O_4$ by WANG et al [14], the broad Raman band $v_6$ at about 640 $cm^{-1}$ is attributed to the partial position disorder of the cations in the spinel structure, i.e., so-called antisite defect.

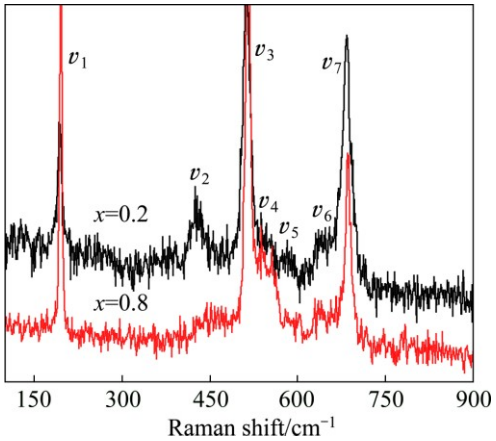


**Fig. 4** Raman spectra of $Ni_{1-x}Co_xCr_2O_4$ ($x$=0.2 and 0.8)

**Table 1** Raman absorption peaks of $Ni_{1-x}Co_xCr_2O_4$

| $x$ | $v_1$/ $cm^{-1}$ | $v_2$/ $cm^{-1}$ | $v_3$/ $cm^{-1}$ | $v_4$/ $cm^{-1}$ | $v_5$/ $cm^{-1}$ | $v_6$/ $cm^{-1}$ | $v_7$/ $cm^{-1}$ |
|---|---|---|---|---|---|---|---|
| 0.2 | 192 | 425 | 512 | 538 | 582 | 640 | 684 |
| 0.8 | 195 | 449 | 513 | 540 | 556 | 635 | 687 |

### 3.5 Magnetic properties

The thermal magnetization of $Ni_{0.8}Co_{0.2}Cr_2O_4$ and $Ni_{0.2}Co_{0.8}Cr_2O_4$ with different $Co^{2+}$ contents are carried out with the temperature ranging from 5 to 200 K at a magnetic field of $4\times10^4$ A/m, as shown in Fig. 5. The magnetization of $Ni_{0.8}Co_{0.2}Cr_2O_4$ decreases slowly with the temperature ranging from 5 to 31 K, then decreases sharply to the paramagnetic region at $T_C$=73 K, which is the Curie temperature. For $Ni_{0.2}Co_{0.8}Cr_2O_4$, the magnetization decreases slowly with the temperature ranging from 5 to 25 K, and then increases smoothly to a maximum at about 65 K. Two transitions are visible at $T_s$=25 K and $T_C$=90 K. Below $T_C$=90 K, the spin is long-range linearly ferrimagnetically ordered. A short-range-ordered spiral magnetic structure transforms into a conical magnetic structure at $T_s$=25 K [6]. Figure 5 shows that the value of $T_C$ increases with the substitution

of Co ions for Ni ions. The replacement of Ni by Co ions leads to a change of the radii at the A site and B site. It alters the magnitude of the well-known super-exchange interaction, resulting an increase of the value of $T_C$ with the increasing cobalt content [15]. The saturation magnetization ($M_s$), coercivity ($H_c$), the Curie temperature ($T_C$), the transition temperature for linear to conical alignment ($T_s$) are listed in Table 2. Figure 6 shows the magnetization curves of $Ni_{1-x}Co_xCr_2O_4$ ($x$=0.2, 0.8) at 5 K. The unsaturation magnetization of both $Ni_{0.8}Co_{0.2}Cr_2O_4$ and $Ni_{0.2}Co_{0.8}Cr_2O_4$ at $5.57\times10^4$ A/m is consistent with the conical alignment of the magnetic moments. Both $H_c$ and $M_s$ decrease with the increasing cobalt content. The decrease of $M_s$ can be explained on the basis of the Neel two sub-lattice model [16]. The net magnetization can be expressed as: $M_{cal}=M_B(x)-M_A(x)$, where $M_A$ and $M_B$ are the magnetic moments at A site and B site, respectively. The magnetic moments are calculated with $\mu=2\sqrt{S(S+1)}\mu_B$, where $S$ is the total spin. Using this formula, it leads to $\mu(Cr^{3+})=\mu(Co^{2+})=3.8\,\mu_B$, and $\mu(Ni^{2+})=2.8\,\mu_B$. The calculated values $M_{cal}$ are also listed in Table 2. Even though it is much higher than the measured $M_s$, probably due to the unsaturated magnetization of the conically aligned magnetic moments, the calculated magnetizations reflect the decreasing trend with the Co substitution.

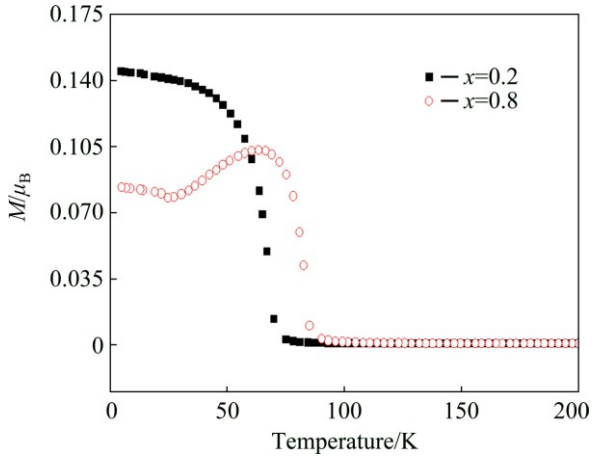


**Fig. 5** Temperature-dependent magnetization measured with external magnetic field of 0.05 T for $Ni_{1-x}Co_xCr_2O_4$ ($x$=0.2 and 0.8)

**Table 2** Magnetic parameters of $Ni_{1-x}Co_xCr_2O_4$

| $x$ | $M_s/\mu_B$ | $H_c$/T | $M_{cal}/\mu_B$ | $T_C$/K | $T_s$/K |
|---|---|---|---|---|---|
| 0.2 | 0.31 | 1.17 | 4.6 | 79 | – |
| 0.8 | 0.25 | 0.57 | 4 | 91 | 25 |

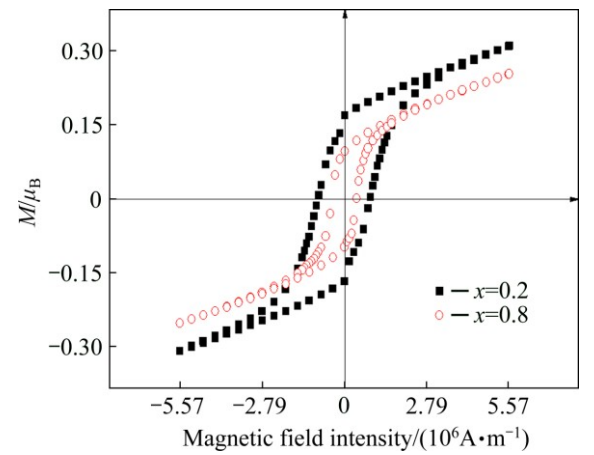


**Fig. 6** Magnetization hysteresis of $Ni_{1-x}Co_xCr_2O_4$ ($x$=0.2 and 0.8) at 5 K

## 4 Conclusions

1) Polycrystalline $Ni_{1-x}Co_xCr_2O_4$ ($x$=0, 0.05, 0.1, 0.15, 0.2, 0.3, 0.5, 0.7, 0.8, 0.85, 0.9, 0.95, 1.0) were synthesized by solid-state reaction. The XRD pattern shows that the $NiCr_2O_4$ has the tetragonal structure with the space group $I4_1/amd$. However, the structure of $Ni_{1-x}Co_xCr_2O_4$ with $x\geq0.05$ is cubic with the space group $Fd\bar{3}m$.

2) The UV-Vis bands $\lambda_3$, $\lambda_4$, $\lambda_5$ and $\lambda_6$ suggest that the Co ions locate at the A site, and the Cr ions locate at the B site in $Ni_{1-x}Co_xCr_2O_4$. The weak UV-Vis absorption at about 415 $cm^{-1}$, the FT-IR peak at about 600 $cm^{-1}$, and the broad Raman band at about 640 $cm^{-1}$, indicate that some of the Co ions enter the B site. Therefore, although the Co ions primarily occupy the A site, a minor part of them enter into the B site in the $Ni_{1-x}Co_xCr_2O_4$ compounds.

3) The Curie temperatures are 75 K and 90 K for the compounds with $x$=0.2 and 0.8, respectively. The replacement of Ni by Co ions leads to a change of the radii at the A site and B site. This alters the magnitude of the well-known super-exchange interaction, resulting in an increase of the value of $T_C$ with the increasing cobalt content.

## References

[1] MOUSAVI Z, ESMAEILI-ZARE M, SALAVATI-NIASARI M. Magnetic and optical properties of zinc chromite nanostructures prepared by microwave method [J]. Transactions of Nonferrous Metals Society of China, 2015, 25: 3980−3986.

[2] LUO Guang-sheng, ZHOU Wei-ping, LI Jian-de, JIANG Gui-wen, TANG Shao-long, DU You-wei. Effect of Cu ion substitution on structural and dielectric properties of Ni−Zn ferrites [J]. Transactions of Nonferrous Metals Society of China, 2015, 25: 3678−3684.

[3] BARMAN J, RAVI S. Study of exchange bias behavior in $Ni(Cr_{1-x}Fe_x)_2O_4$ [J]. Solid State Communications, 2015, 201: 59−63.

[4] KOCHUR A G, KOZAKOV A T, GOOGLEV K A, MIKHEYKIN A S, TORGASHEV V I, BUSH A A, NIKOLSKII A V. Chemical bonding and valence state of 3d-metal ions in $Ni_{1-x}Co_xCr_2O_4$ spinels from X-ray diffraction and X-ray photoelectron spectroscopy data [J]. Journal of Electron Spectroscopy and Related Phenomena, 2014, 195: 208−219.

[5] PTAK M, MACZKA M, GAGOR A, PIKUL A, MACALIK L, HANUZA J. Temperature-dependent XRD, IR, magnetic, SEM and TEM studiesof Jahn–Teller distorted $NiCr_2O_4$ powders [J]. Journal of Solid State Chemistry, 2013, 201: 270−279.

[6] MUFTI N, NUGROHO A A, BLAKE G R, PALSTRA T T M. Magnetodielectric coupling in frustrated spin systems: The spinels $MCr_2O_4$ (M = Mn, Co and Ni) [J]. Journal of Physics, 2010, 22: 075902.

[7] GINGASU D, MINDRU I, CULITA D C, PATRON L, CALDERON-MORENO J M, OSICEANU P, PREDA S, OPREA O, PARVULESCU V, TEODORESCU V, WALSH J P S. Structural, magnetic and catalytic properties of cobalt chromite obtained through precursor method [J]. Materials Research Bulletin, 2015, 62: 52−64.

[8] EWAIS E M M, BESISA D H A, El-AMIR A A M, El-SHEIKH S M, RAYAN D E. Optical properties of nanocrystalline magnesium aluminate spinel synthesized from industrial wastes [J]. Journal of Alloys and Compounds, 2015, 649: 159−166.

[9] GABAL M A, KOSA S, ALMUTAIRI T S. Cr-substitution effect on the structural and magnetic properties of nano-sized $NiFe_2O_4$ prepared via novel chitosan route [J]. Journal of Magnetism and Magnetic Materials, 2014, 356: 37−41.

[10] ZAYAT M, LEVY D. Blue $CoAl_2O_4$ particles prepared by the sol-gel and citrate-gel methods [J]. Chemistry of Materials, 2000, 12: 2763−2769.

[11] LI Shan-dong, BI Hong, TIAN Zong-jun, XU Feng, GU Ben-xi, LU Mu, DU You-wei. Surface spin pinning effect of polymer decomposition residues in $CoCr_2O_4$ nanocrystallites system [J]. Journal of Magnetism and Magnetic Materials, 2004, 281: 11−16.

[12] WANG Zhong-wu, SAXENA S K, LAZOR P, O'NEILL H S C. An in situ Raman spectroscopic study of pressure induced dissociation of spinel $NiCr_2O_4$ [J]. Journal of Physics and Chemistry of Solids, 2003, 64: 425−431.

[13] SUCHOMSKI C, REITZ C, BREZESINSKI K, SOUSA C T, ROHNKE M, IIMURA K, ARAUJO J P E, BREZESINSKI T. Structural, optical, and magnetic properties of highly ordered mesoporous $MCr_2O_4$ and $MCr_{2-x}Fe_xO_4$ (M = Co, Zn) spinel thin films with uniform 15 nm diameter pores and tunable nanocrystalline domain sizes [J]. Chemistry of Materials, 2012, 24: 155−165.

[14] WANG Zhong-wu, LAZOR P, SAXENA S K, ARTIOLI G. High-pressure raman spectroscopic study of spinel ($ZnCr_2O_4$) [J]. Journal of Solid State Chemistry, 2002, 165: 165−170.

[15] GABAL M A, EL-SHISHTAWY R M, ANGARI Y M A. Structural and magnetic properties of nano-crystalline Ni−Zn ferrites synthesized using egg-white precursor [J]. Journal of Magnetism and Magnetic Materials, 2012, 324: 2258−2264.

[16] SERTKOL M, KOSEOGLU Y, BAYKAL A, KAVAS H, BOCKURT A, TOPRAK M S. Microwave synthesis and characterization of Zn-doped nickel ferrite nanoparticles [J]. Journal of Alloys and Compounds, 2009, 486: 325−329.

# 反位紊乱 $Ni_{1-x}Co_xCr_2O_4$ 尖晶石的光学特性与磁学特性

高 玉，常 虹，武 强，王宏艳，庞艳波，刘 芳，朱宏静，云月厚

内蒙古大学 物理科学与技术学院，呼和浩特 010021

**摘 要**：通过对化合物 $Ni_{1-x}Co_xCr_2O_4$ 的紫外吸收光谱，红外吸收光谱和拉曼光谱分析，说明 Co 离子中绝大多数占据了四面体(A)位置，少部分占据了八面体（B）位置。Co 离子占位紊乱是由于八面体中 Co 离子的半径($r$=0.65 Å)接近于八面体中 Cr 离子的半径($r$=0.62 Å)引起的。随着 Co 含量的增加，在 510 $cm^{-1}$ 附近出现的红外吸收峰向高频方向移动，这是由于 Co 离子替代四面体中 Ni 离子使八面体中阳离子与氧之间的距离减小，导致键能增强引起的。磁性测量展示了 $x$=0.2 和 0.8 的居里温度($T_C$)分别为 75 K 和 90 K。

**关键词**：尖晶石；反位缺陷；电子跃迁；光学性能；磁学性能

**(Edited by Yun-bin HE)**